Biosensors and Bioelectronics 81 (2016) 445–453

Contents lists available at ScienceDirect

Biosensors and Bioelectronics

journal homepage: www.elsevier.com/locate/bios

$FeMoO_4$ based, enzyme-free electrochemical biosensor for ultrasensitive detection of norepinephrine ☆

Kunda J. Samdani [a,1], Jitendra S. Samdani [a,1], Nam Hoon Kim [a], Joong Hee Lee [a,b,*]

[a] Department of BIN Convergence Technology, Chonbuk National University, Jeonju, Jeonbuk 561-756, Republic of Korea
[b] Center for Carbon Composites Materials, Department of Polymer & Nano Science and Technology, Chonbuk National University, Jeonju, Jeonbuk 561-756, Republic of Korea

ARTICLE INFO

Article history:
Received 17 January 2016
Received in revised form
8 March 2016
Accepted 14 March 2016
Available online 15 March 2016

Keywords:
Norepinephrine
$FeMoO_4$
Nanorods
Fe (II)-Dioxygen complex
Electrochemical
Biosensor

ABSTRACT

Herein, $FeMoO_4$ (FM) nanorods were synthesized by a template-free, facile, hydrothermal method in an aqueous medium. The surface morphology of $FeMoO_4$ was identified with field emission scanning electron microscopy (FESEM) and transmission electron microscopy (TEM). X-ray diffraction (XRD) was performed to identify the crystallographic nature of the as-synthesized $FeMoO_4$. The as-synthesized material was used as an active electrode material for the oxidation of a neurotransmitter (i.e. norepinephrine (NE)) by cyclic voltammetry (CV) and differential pulse voltammetry (DPV) techniques. $FeMoO_4$ possesses polycrystallanity and bimetallic character, which helps to enhance the performance of the FM/GCE as compared to the GCE. The enhanced performance was also due to the formation of Fe (II)-dioxygen complexes, which catalyze the oxidation of NE. Meticulous observations taken from CV studies proved the diffusion-controlled nature of the reaction with a diffusion coefficient of 1.10×10^{-4} cm^2/s and a standard heterogeneous rate constant of 4.078×10^{-3} cm/s. The amperometric response of NE on the FM/GCE showed a linear increase in the current between 5.0×10^{-8} M and 2.0×10^{-4} M with a detection limit of 3.7×10^{-9} M. In the amperometric study, the time required to reach the 98% steady state response, after successive additions of 50 nM NE, was less than 3 s. The FM/GCE showed good sensitivity, and stability for the determination of NE.

1. Introduction

Norepinephrine (NE) is a crucial catecholamine neurotransmitter in the mammalian central nervous system. Extremely abnormal concentrations of NE may lead to the occurrence of a variety of diseases, such as ganglion neuronal, ganglia neuroblastoma, paraganglioma, and Parkinson's disease (Ardakani et al., 2011). In addition, NE accelerates human immunodeficiency virus-1 (HIV-1) replication via protein kinase because NE enhances the adhesion of HIV-1 infected leukocytes to cardiac microvascular endothelial cells (Cole et al., 1998). Therefore, it is necessary to develop sensitive, selective, and reliable methods for the direct determination of trace amounts of NE due to its physiological functions and the diagnosis of certain diseases in clinical medicine.

Despite the fact that several techniques are available for the determination of NE including HPLC (Sabbioni et al., 2004), spectrophotometry (Zhu et al., 1997) and fluorometry (Oka et al., 1982), electrochemical methods (Wei et al., 2002; Lu et al., 2004; Liu et al., 2008; Bian et al., 2010; Ardakani et al., 2010; Goyal et al., 2011; Li et al., 2012; Beitollahi and Mohammadi, 2013; Chen et al., 2015) have several advantages over other methods such as their low cost, simpler procedures, high sensitivity, and reproducibility. NE is an electroactive compound that can be oxidized electrochemically; therefore, the development of electrochemical sensors for the determination of NE has been the focus of research over the past decade. However, few reports have been published on the use of modified carbon materials as effective electrodes for NE sensing. Liu et al. (2008) reported the use of a poly-calconcarboxylic acid modified carbon electrode, and Beitollahi and Mohammadi (2013) used carbon paste electrode (CPE) modified with 5-mino-3′,4′-dimethyl-biphenyl-2-ol (5ADB) for the selective determination of NE with a detection limit of 0.01 and 0.59 μM respectively. Bian et al. (2010) investigated the electrochemical response of NE with carbon-coated nickel magnetic nanoparticle modified glassy carbon electrode. However, the fabrication of these electrodes is

☆Electronic supplementary information (ESI) available.

* Corresponding author at: Center for Carbon Composites Materials, Department of Polymer & Nano Science and Technology, Chonbuk National University, Jeonju, Jeonbuk 561-756, Republic of Korea.
E-mail address: jhl@jbnu.ac.kr (J.H. Lee).

[1] Both authors contributes equal.

http://dx.doi.org/10.1016/j.bios.2016.03.029
0956-5663/

tedious and the detection limit of NE is not appreciable. Wang (2008) reported that nanomaterial modified electrodes can reduce the potential, improve the electrochemical reaction rate, and increase the selectivity of the modified electrodes. Hence, researchers are currently focused on using nanomaterials, like metal oxides, bi-metallic oxides, and nanocomposites, as enzyme-free biosensor electrode materials. Recently, Ardakani et al. (2010) and Li et al. (2012) studied the electrochemical detection of NE with metal oxide nanoparticles (e.g., ZrO_2 and WO_3–TiO_2); however, the sensitivity of the electrode was not satisfactory. Alternatively, binary metal oxides are also considered to be potential materials for electrochemical applications, including high-performance supercapacitors (Zhang and Lou, 2013), lithium ion batteries (Cherian et al., 2013), and sensors (Zhang et al., 2015a, 2015b), because of their feasible oxidation state and high electrical conductivity. Recently, metal molybdates, such as $CoMoO_4$ (Liu et al., 2013), $NiMoO_4$ (Zhang et al., 2015a, 2015b; Cai et al., 2013), $MnMoO_4$ (Senthilkumar et al., 2015) $BaMoO_4$ (Yang et al., 2011), and $FeMoO_4$ (Ju et al., 2015; Zhang et al., 2010; Cui et al., 2012) have been extensively studied for electrochemical applications. Among them, $FeMoO_4$ is one of the most important metal molybdates and is expected to offer richer redox chemistry compared to single component oxides due to its combined contributions from both iron and molybdenum ions (Mai et al., 2011; Wang and Wang, 2013). $FeMoO_4$ has been employed in the large-scale production of formaldehyde by the partial oxidation of methanol in an excess of oxygen (air) at relatively low temperatures (Soares et al., 2001; Soderhjelm et al., 2008). $FeMoO_4$ has also been used as an effective electrode material for Li-ion batteries (Leyzerovich et al., 2004; Xiao et al., 2010). Most recently, Liu et al. (2015) synthesized rose-shaped $FeMoO_4$ in a glycerol solvent and used these materials as biosensors for hydrogen peroxide; however, the sensitivity towards H_2O_2 is limited to 0.5 μM. Nevertheless, inadequate data is available on their use as an electrode material for biosensors.

Therefore, the present study was carried to establish a facile, template-free synthesis method for $FeMoO_4$ (FM) nanorods. To the best of our knowledge, this is the first report investigating the application of as-synthesized $FeMoO_4$ nanorods as biosensors for the effective oxidation of norepinephrine.

2. Material and methods

2.1. Reagents and materials

Norepinephrine (NE), ascorbic acid (AA), uric acid (UA), Nafion (Nf), ferrous sulfate, Na_2HPO_4, NaH_2PO_4 and sodium molybdate were purchased from Sigma Aldrich. A buffer solution (PBS, 0.2 M, pH=7.2) was prepared from NaH_2PO_4 and Na_2HPO_4. De-ionized water was used throughout the experiments.

2.2. Synthesis and characterization of $FeMoO_4$ nanorods

In a typical synthesis of $FeMoO_4$ nanorods, 0.36 M $FeSO_4 \cdot 7H_2O$ and 0.12 M Na_2MoO_4 were dissolved in double distilled water. The detail of material synthesis and characterization has been explained in Supplementary information.

2.3. Fabrication of electrodes and electrochemical measurements

All electrochemical experiments were performed on a CHI 660 D electrochemical work station (CHI Instruments Co., Austin, USA) with a conventional three-electrode system comprised of a platinum wire (auxiliary electrode), Ag/AgCl (reference electrode), and a modified or unmodified glassy carbon electrode (GCE) (3 mm in diameter, as the working electrode). Prior to modification, the GC electrode was polished with 0.50 mm alumina slurry and rinsed thoroughly with water. The electrode was then sonicated in deionized water for 30 min to remove any adsorbed alumina particles. The as-prepared $FeMoO_4$ nanorods were dispersed in 1 mL of a 0.1% Nafion solution (10 mg/mL). The above suspensions (20 μL) were dropped onto the clean GCE and dried at room temperature. The three electrodes were then rinsed twice with deionized water and used in the binding and selective recognition experiments. CV and DPV measurements were carried out by repeated potential scanning between −0.2 and 0.7 V at a scan rate of 30 mV/s.

3. Results and discussion

3.1. Characterization

XRD was employed to characterize the crystal phase of the as-prepared material. The typical XRD spectrum of the sample is shown in Fig. 1a. All peaks could be readily indexed to monoclinic β-$FeMoO_4$ with lattice constants of a=10.29 A°, b=9.39 A°, c=7.07 A°, and β=106.31 A°. These match well with the standard XRD pattern for monoclinic β-$FeMoO_4$ (JCPDS card no. 089-2367). The monoclinic structure of the β-$FeMoO_4$ crystals has a wolframite-type structure with point group symmetry C2/m and two clusters per unit cell (Z=2). In these unit cells, the Fe and Mo atoms are coordinated to six oxygen atoms, which form distorted octahedral [FeO_6] and [MoO_6] clusters (Ju et al., 2015). The XRD pattern shows that the as-prepared material is polycrystalline in nature; this is further confirmed by HRTEM analysis. Fig. 1b shows the Raman spectra of the as-synthesized $FeMoO_4$ nanorods. A prominent peak at 926 cm^{-1} can be seen in the Raman spectra; this was assigned to the 2Ag components. Two peaks between 800 and 900 cm^{-1} were assigned to the υ3 component, which may be due to the high fluorescent background present in $FeMoO_4$ (Saleem, 1987). The frequencies observed in the region between 310 and 480 cm^{-1} in the Raman spectrum were assigned to the bending modes of Mo–O bonds. Fig. 1c shows SEM images of the as-prepared $FeMoO_4$ nanorods at different magnifications. At a reaction time of 6 h, well-grown nanorods were observed with an average length of 600–700 nm and an average diameter of 100–150 nm (average aspect ratio is about four to six). Detailed morphological information of the synthesized $FeMoO_4$ nanorods was obtained by HRTEM (Fig. 2). The TEM micrographs of $FeMoO_4$ reveal the formation of nanorods. The SAED pattern of the nanorods exhibits a series of bright rings with a few bright spots, suggesting that they are polycrystalline in nature (inset of Fig. 2b). These results are in agreement with the XRD data. The HR-TEM image of the nanorods (Fig. 2d) reveals an interplanar spacing of 0.68 nm, which is consistent with the (110) plane of the $FeMoO_4$ monoclinic phase, as calculated from the XRD pattern. The EDS analysis shows well-resolved peaks for Fe, Mo, and O. The major peak is attributed to copper, which was used as the substrate (Fig. S1). EDS elemental mapping (Fig. 2e-h) also shows that the distribution of these elements is uniform throughout the nanorod. This may lead to constant current flow during the electrochemical study. Also, there are some small particles/extensions that can be seen on the surface of the nanorods in the SEM (inset of Fig. 1d) and TEM (Fig. 2a and c) images. These may act as precursors for the formation of subsequent nanorods (Zhang et al., 2015a, 2015b).

Obtaining a good understanding of the parameters that control crystallization should enable us to grow nanoparticles of a desired size. Initially, the reaction was carried out at lower temperatures, but this leads to an uneven size distribution in the product. The reaction time was found to be another important factor that influences the final morphology of $FeMoO_4$. Hence, a series of

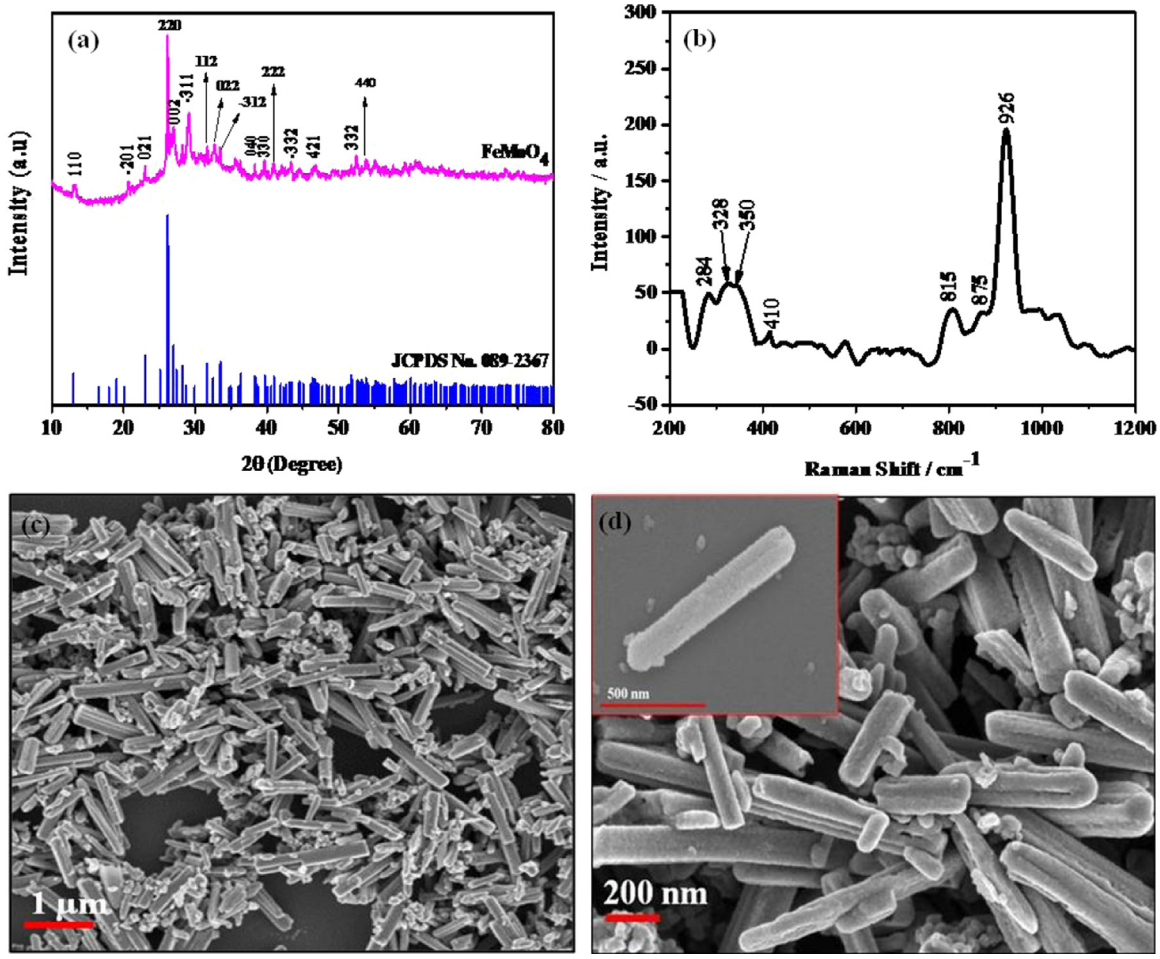

Fig. 1. a) XRD pattern of the as-synthesized $FeMoO_4$ nanorods compared to the standard diffraction pattern of β-$FeMoO_4$, b) Raman spectra of as-synthesized $FeMoO_4$ nanorods, and c) SEM images of the $FeMoO_4$ nanorods at (a) low (30.00 K X), (b) high (100.00 K X) magnification.

reactions was carried out at 3, 6, 9, and 12 h while all of the parameters were kept constant. The proposed growth mechanism of the $FeMoO_4$ nanorods is described below. Initially, $FeMoO_4$ nuclei are formed via a reaction between MoO_4^{2-} ions and Fe^{2+} ions in the solution. After the initial nucleation process, $FeMoO_4$ grains coarsen into nanorods; this was confirmed by changing the reaction time from 3 h to 12 h. By analyzing SEM and TEM images of the products obtained at various reaction times (Fig. S3) it was observed that the nucleation process starts after 3 h, resulting in agglomerates/particles of $FeMoO_4$. These agglomerated particles are amorphous in nature (inset of Fig. S3e), as can be seen from the SAED pattern. Furthermore, these agglomerated nanoparticles developed into nanorods as the reaction time was extended to 6 h. At this stage, surface of the nanorods was rough with nanoparticles attached to their surfaces, and they were polycrystalline in nature (Fig. S3f). After a reaction time of 9 h, the size of the rods increased and they became perfectly crystalline, as can be seen from the SAED pattern (Fig. S3g). As the reaction time was increased further, the nanorods became fused together to form micro rods with an average length of 37 μm and an average diameter of 3.5 μm. They were also so dense that we were unable to obtain an SAED pattern. On the basis of our SEM and TEM results, as well as results found in the literature (Ju et al., 2015; Zhang et al., 2010; Cui et al., 2012), we believe that the formation of the $FeMoO_4$ nanorods can be attributed to the Ostwald ripening process. The minute observation of TEM images also shows that the nanorods coarsen from the inner parts of the material (Fig. 2c and d). Hence, the inner parts of the nanorods become more crystalline than the surface parts. This change in crystallinity as a function of the reaction time was also verified with the XRD patterns (Fig. S2). With this data, the reaction time for the synthesis of $FeMoO_4$ nanorods was optimized at 6 h. Zhang et al. also explained a similar type of growth mechanism; however, they were unable to obtain uniform nanorods. Herein, using our proposed method, one can achieve a desired morphology in an aqueous medium.

3.2. Electrochemical study

Since the early work of Adams et al. (1972), which introduced electrochemistry to the neurosciences, numerous electrochemical techniques and electrode materials have been used to identify and resolve catecholamines. In the present work, for the first time, $FeMoO_4$ nanorods were employed for the electrochemical detection of NE. In order to study the electrochemical behavior of the as-prepared material, CV was carried out with bare GCE and modified electrode i.e. FM/GCE with and without 100 μM NE in 0.2 M PBS (pH=7.2) at a scan rate of 30 mV/s (Fig. 3a). There were no redox peaks in the absence of NE in PBS (pH=7.2) over the potential range between −0.2 and 0.8 V. Furthermore, with bare GCE the oxidation of NE is observed at 0.49 V. Alternatively, with the modified electrode (FM/GCE), a 70 mV shift in the negative direction (0.42 V) was observed in the presence of 100 μM NE. The less positive potential shift might be due to the hydrogen bonding interactions between $FeMoO_4$ and either $–NH_2$ or the –OH functionality of NE. Also, at pH 7.2, NE exists in a cationic form (Gu et al., 1996); hence, electrostatic interactions between the amine

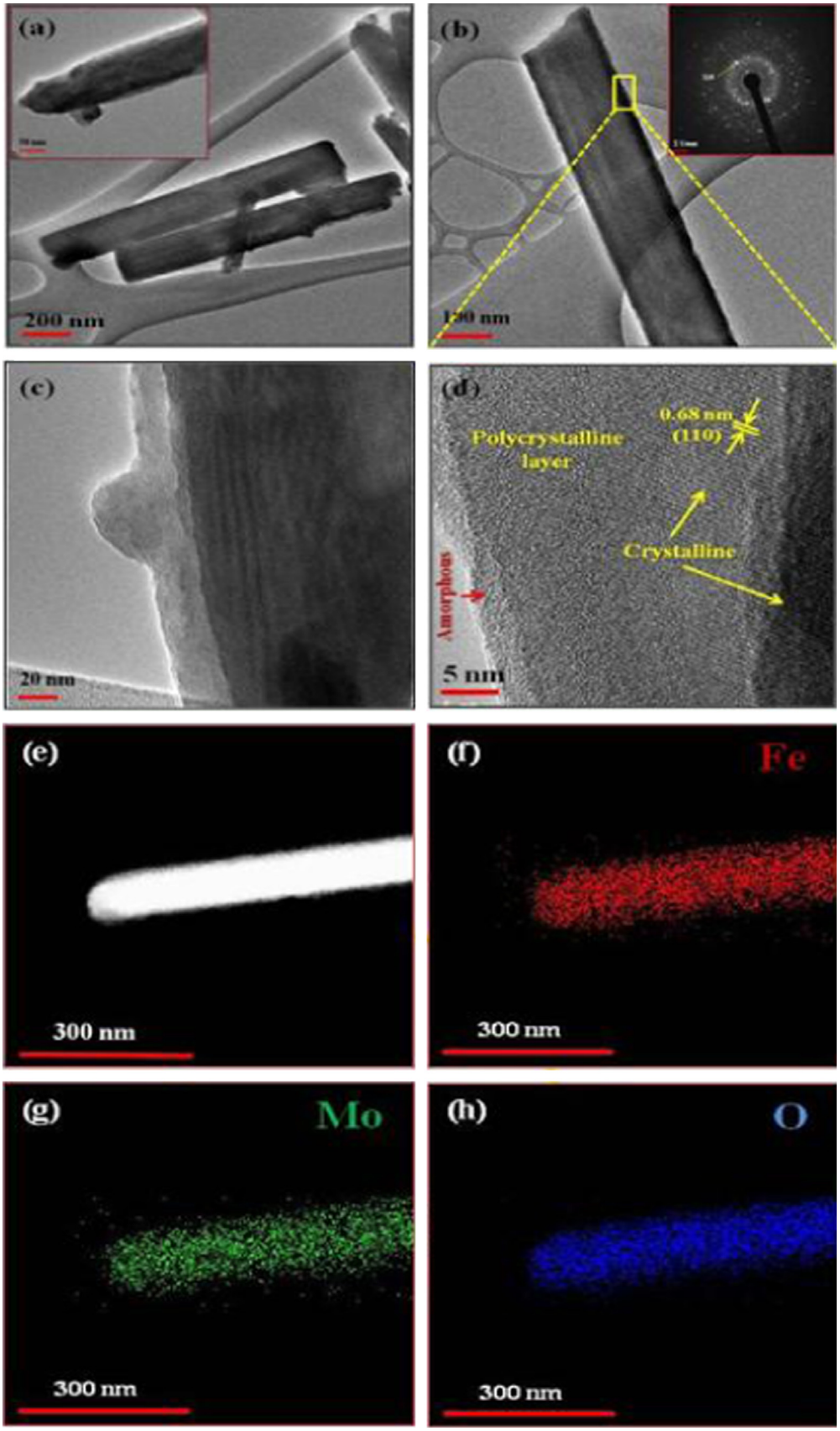

Fig. 2. TEM images of $FeMoO_4$ nanorods (a) at 200 nm, (b) at 100 nm, (c) at 20 nm, and (d) at 5 nm. The inset of b is the electron diffraction pattern of the nanorod. d) HRTEM images of a nanorod with marked lattice fringes, (e) Dark field TEM image of $FeMoO_4$ nanorod, (f) TEM/EDS Fe-k map, (g) TEM/EDS Mo-k map, and (h) TEM/EDS O-k map elements.

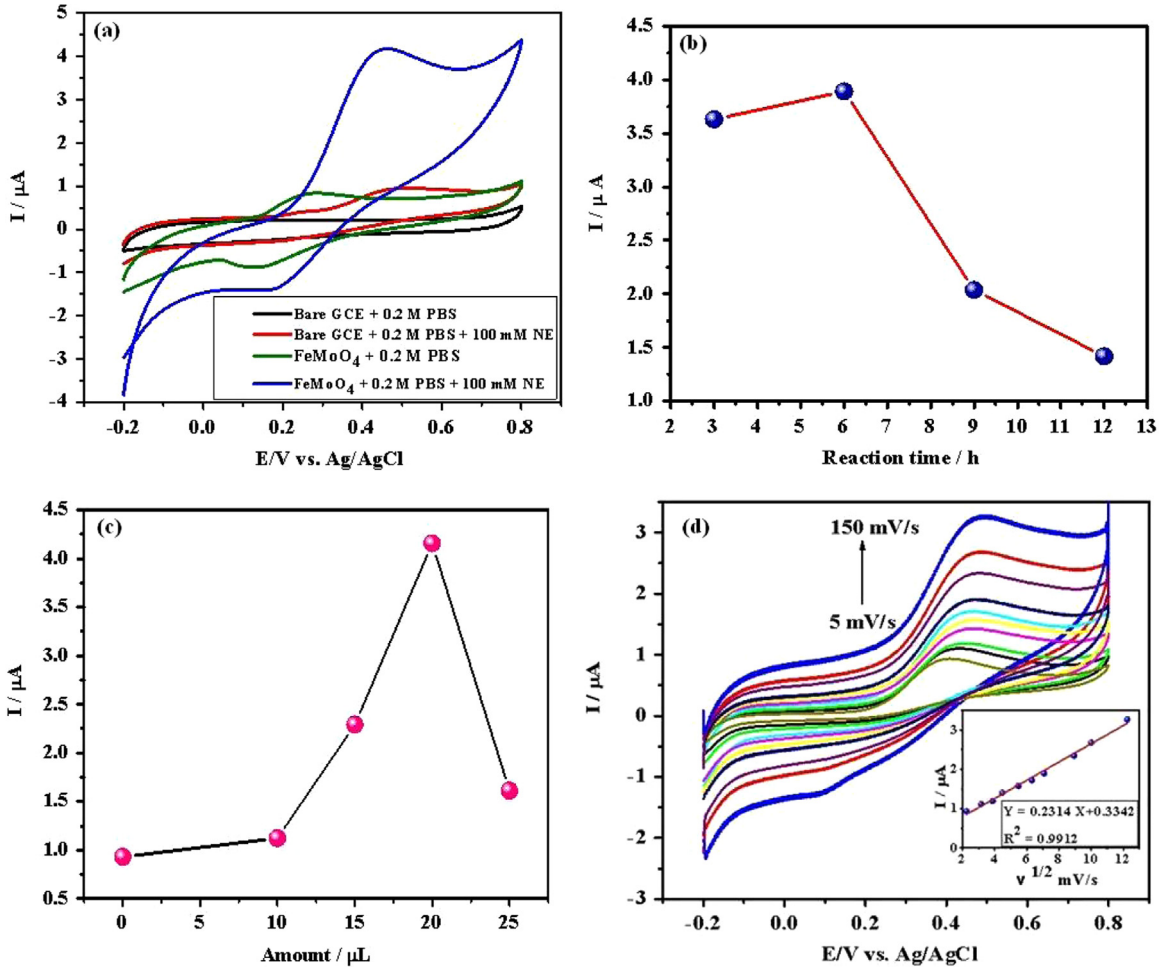

Fig. 3. a) Electrochemical detection of 100 µM NE in 0.2 M PBS (pH=7.2) at a scan rate of 30 mV/s, b) DPV curve of $FeMoO_4$ nanorods at various reaction times in the presence of 100 µM NE in 0.2 M PBS (pH=7.2), c) loading capacity of the electrode with $FeMoO_4$ suspension (10 mg/mL), and d) effect of the scan rate from 5 mV/s to 150 mV/s, in 0.2 M PBS (pH=7.2). The inset of d shows the plot of the peak current vs. $\upsilon^{1/2}$.

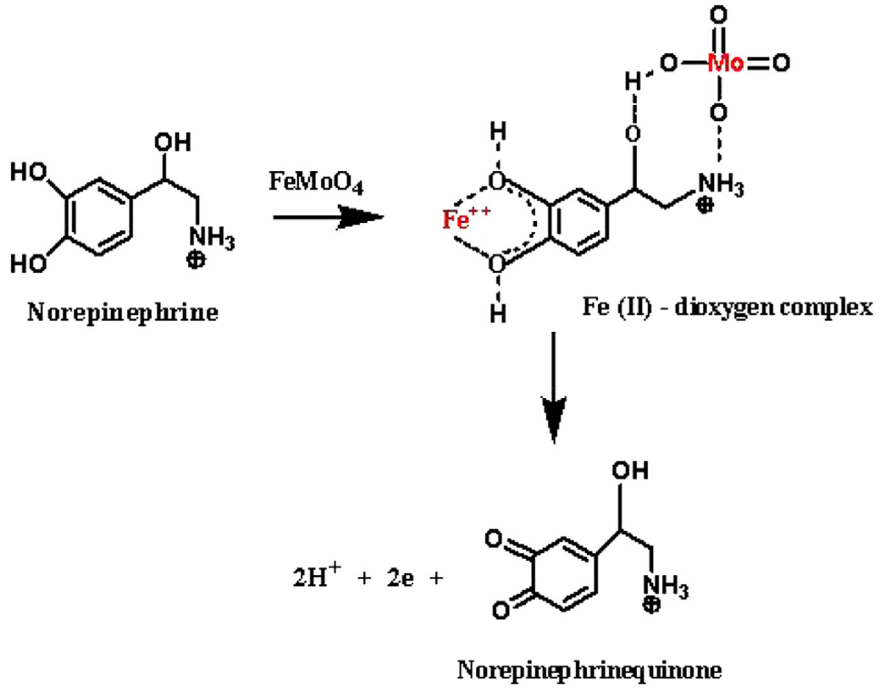

Scheme 1. Schematic presentation of electrochemical oxidation.

groups of NE and the anionic form of $FeMoO_4$ are possible. The cathodic peak current in Fig. 3a shows a great enhancement in the current with the FM/GCE, which provides evidence that $FeMoO_4$ acted as an excellent mediator for electron transfer and possesses very high electrocatalytic activity towards the oxidation of NE. The separation between the peak potentials with the modified electrode, ΔEp (ΔEp=Epc-Epa), was about 240 mV; this is more than the value of 59/n mV at 25 °C expected for the reversible reaction (Bard and Faulkner, 2001). In the CV curve, the reduction peak shows a decrease in the current which may be due to the formation of norepinephrinequinone as shown in Scheme 1. Additionally, the electrochemical behavior of as-prepared $FeMoO_4$ nanorods at various times (3, 6, 9 and 12 h) in presence of 100 μM NE in 0.2 M PBS (pH=7.2) was studied with DPV technique. Fig. 3b reveals that the $FeMoO_4$ nanorods synthesized at 6 h show the maximum current in the presence of 100 μM NE in 0.2 M PBS (pH=7.2). This may be due to the polycrystalline nature of the material, which gives an effective path for electron transport. This effect could be less significant in the case of amorphous or highly crystalline materials. Therefore, further electrochemical studies were carried out for the $FeMoO_4$ nanorods synthesized at 6 h. The loading capacity of the FM/GCE was also evaluated with CV with loadings of 10 μL, 15 μL, 20 μL, and 25 μL suspensions of $FeMoO_4$ (10 mg/mL). The obtained results showed that the peak current of NE increases as the material loading increases up to 20 μL and then suddenly drops at 25 μL (Fig. 3c). NE showed a high oxidation current when 20 μL of $FeMoO_4$ was loaded onto the GCE. Thus, a loading value of 20 μL was used in the remainder of the experiment.

To understand the nature of the oxidation reaction of NE at the FM/GCE, CV was carried out at different scan rates from 5 mV/s to 150 mV/s. The effect of the potential scan rate (ν) on the electrochemical properties of the FM/GCE with 0.2 M PBS containing 50 μM NE was studied by CV (Fig. 3d). The plot of the cathodic peak currents (Ip) linearly increases with the square root of the scan rate [linear equation, I (μA)=0.2314 $\nu^{1/2}$ [(mV/s)$^{1/2}$]+0.3342, R^2=0.9912] in the range of 5–150 mV/s (inset of Fig. 3d), indicating that the redox process at the modified electrode is diffusion-controlled in nature with two electrons and two protons (Bard and Faulkner, 2001). It also demonstrates that the redox process at the modified FM/GCE is a surface-confined process with quick electron transfer kinetics. Based on the Ip vs. $\upsilon^{1/2}$ plot the diffusion coefficient (D) of NE (cm^2/s) was calculated using the Randles–Sevcik Eq. (1) (Nie et al., 2010):

$$i_p = (2.69 \times 10^5) n^{2/3} A D^{1/2} C \nu^{1/2} \quad (1)$$

Here, i_p is the peak current, n is the number of electrons, A is the electrode area (cm^2), D is the diffusion coefficient (cm^2/s), C is the redox molecule concentration (mol/cm^3), and υ is the potential sweep rate (V/s). Clearly, i_p varies proportionally with A, C, and $\upsilon^{1/2}$. These relationships hold when the charge-transfer kinetics are relatively rapid. The estimated value of D at the GCE was found to be 4.03×10^{-6} cm^2/s, whereas at the FM/GCE the value of D was 1.10×10^{-4} cm^2/s. Furthermore, the standard heterogeneous rate constant (k_s) values for NE at the GCE and FM/GCE were calculated using the Velasco Eq. (2) (Velasco, 1997):

$$k_s = 1.11\, D^{1/2} (E_p - E_{p/2})^{-1/2} \nu^{1/2} \quad (2)$$

Here, k_s is the standard heterogeneous rate constant, D is the diffusion coefficient, E_p is the oxidation peak potential, $E_{p/2}$ is the half-wave oxidation peak potential, and υ is the scan rate. The K_s value obtained for the GCE was 7.08×10^{-4} cm/s and the K_s value of the FM/GCE was 4.078×10^{-3} cm/s. The higher k_s value for NE at the FM/GCE indicates that the oxidation of NE was faster than at the bare GCE. A plot of the scan rate normalized current ($i/\nu^{1/2}$) vs. the scan rate (Fig. S4) exhibits the shape that is characteristics of a typical electrocatalytic (EC) process (Bard and Faulkner, 2001). The rate determining step of the reaction estimated by the Tafel slope (b) can be obtained from the slope of Ep vs. log υ (Fig. S5) using Eq. (3) (Harrison and Khan, 1970):

$$E_p = \frac{b}{2} \log \nu + \text{Constant} \quad (3)$$

Here, υ is the scan rate and 'b' is the Tafel slope. Additionally, the Tafel slope can also be written as:

$$b = \frac{2.3\, RT}{\alpha n F} \quad (4)$$

The number of electrons involved in the rate-determining step can be estimated from the slope of the Tafel plot. The value of the Tafel slope was found to be 93 mV (Fig. S5), which indicates that a one-electron transfer process is the rate-determining step (RDS); this has a charge transfer coefficient (α) of about 0.63.

In this study, NE was used as a model to investigate the application and mechanism of $FeMoO_4$ nanorods in neurotransmitter monitoring. Herein, $FeMoO_4$ nanorods showed its robust ability for electron transfer to the electrode surface. Fig. 3a presents a pair of well-defined redox peaks corresponding to the direct electrochemistry of NE on modified FM/GCE electrode. The detailed oxidation mechanism is shown in Scheme 1. Basically, NE contains catechol residue and a side-chain amine group which are capable of coordinating metal ions. On the other side, the as-synthesized material ($FeMoO_4$) exists in the $Fe^{2+}$and MoO_4^{2-} form. When NE was immobilized on the FM/GCE, the Fe^{2+} bound with the dioxygen of catechol residue and formed the Fe (II)-dioxygen complexes (Sigel et al., 2006). Further, the side chain amine group also reacted with $FeMoO_4$ by the electrostatic interactions with MoO_4^{2-} (Gu et al., 1996) and led to the formation of ligand-metal ion-dioxygen complex. Further this complex broke down into norepinephrine-quinone via a two electron process (Lu et al., 2004; Bian et al., 2010; Chen et al., 2015). The formation of Fe (II)-dioxygen complexes led to an increase in the oxidation current in the CV curve whereas the reduction peak showed a decrease in the current intensity due to the formation of quinone. Kannan et al. (2016) also reported that the Fe from bimetallic Ni-Fe nanoparticle system, acted as a synergistic catalyst to enhance the electrocatalytic oxidation of glucose.

The accumulation potential (Eacc) was determined by differential pulse voltammetry (DPV) in the presence of 10 μM NE from −0.2 to 0.7 V (Fig. S6). It was observed that when the accumulation potential was 0.33 V, the peak current reached its maximum. Hence, a potential of 0.33 V was chosen for further analysis using DPV and amperometric techniques. DPV was used for the determination of NE at the modified electrode because of its higher current sensitivity and better resolution compare to CV. The DPV measurement was carried out in 0.2 M PBS (pH=7.2) by repeated potential scanning between 0.0 and 0.7 V. Fig. 4a shows that the DPV peak current responses towards NE were higher at the modified FM/GCE; this indicates better immobilization and a superior binding capacity for the template molecules. The oxidation of NE occurred at 0.33 V, with a well defined inverted 'V'-shaped voltammogram and a stable response. As shown in Fig. 4b, the calibration curves for NE detection by DPV are linear from 1 μM to 167 μM and have the equation Y=0.0067X+0.2706 (R^2=0.9976).

Fig. 5 shows the typical amperometric response curve (i-t curve) towards the oxidation of NE at the FM/GCE in 0.2 M PBS that is obtained by applying a potential of 0.33 V. Sequential additions of 50 nM of NE to the electrode provoked dramatic increases in the current, and the time required to reach the 98% steady state response was less than 3 s (inset of Fig. 5a) upon further additions of 50 nM NE at intervals of 50 s. This biosensor

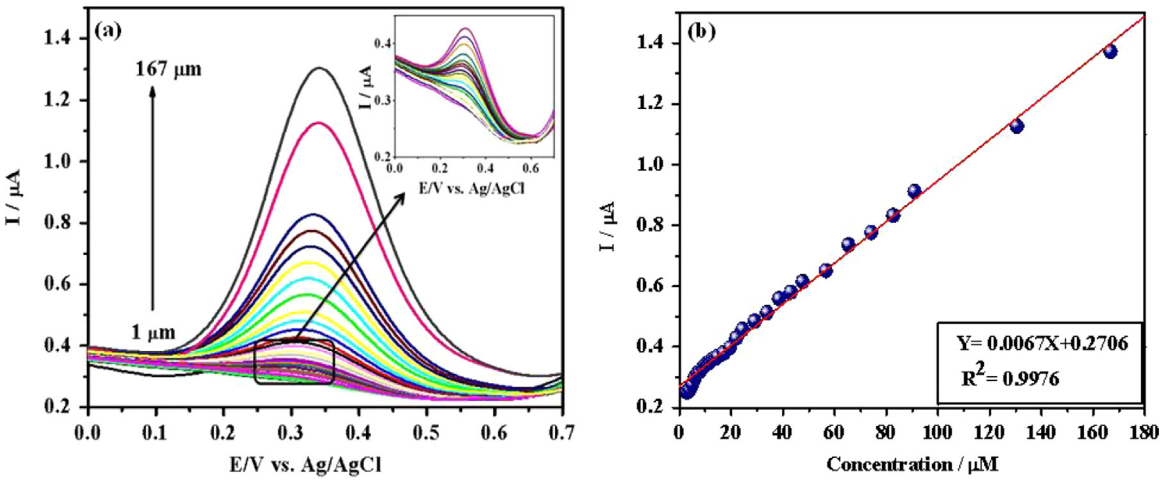

Fig. 4. a) DPV curves for different concentration of NE (1–167 µM) on the FM/GCE. b) Linear relationship between the current and concentration of NE.

yielded a linear response for NE concentrations between 50 nm and 900 nM and had a correlation coefficient of 0.9987, as presented in the inset of Fig. 5a. This sensor also yielded a very low detection limit of 3.7×10^{-9} M estimated at a signal-to-noise ratio of three, without any chemical modifier. Fig. 5b shows that the amperometric current response increased linearly with increasing NE concentrations between 5.0×10^{-8} M and 2.0×10^{-4} M with a correlation coefficient of 0.9989 (inset of Fig. 5b). It is well known that NE is generally present in human blood and urine with the normal concentration ranges of 3×10^{-9}–9×10^{-8} M and 1.7×10^{-7}–7×10^{-7} M, respectively. In this study, it is proven that the material under study can effectively detect the amount of NE from blood and urine as its limit of detection is 3.7×10^{-9} M with wide linear range. This proves that the FM/GCE is suitable for the detection of NE at very low concentrations. It is worth comparing the detection limit of NE that was obtained in the present study with previously reported values for different modified electrodes (Table 1). Table 1 shows that the present FM/GCE had the lowest

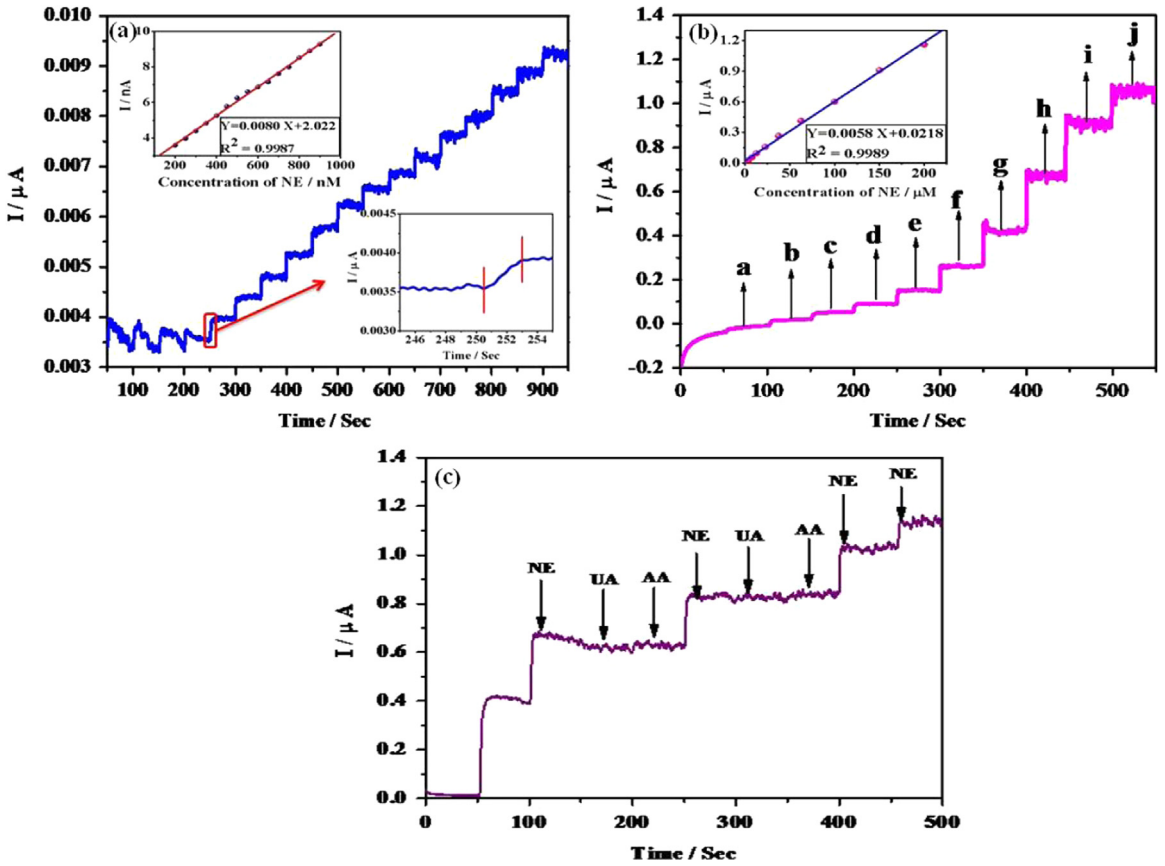

Fig. 5. a) Amperometric i–t curve for the determination of NE at the FM/GCE in a 0.2 M PBS. Inset (a): Plot of the concentration of NE vs. current and plot of the current vs. time, showing a steady state current within 3 s. (b) Amperometric i–t curve for the determination of NE at the FM/GCE in a 0.2 M PBS. (Each addition increases the concentration to (a) 1, (b) 3.5, (c) 7.5, (d) 12.5, (e) 22.5, (f) 37.5, (g) 62.5, (h) 100, (i) 150, and (j) 200 µM NE at the FM/GCE in a 0.2 M PBS at a intervals of 50 s. Inset (b): Plot of the concentration of NE vs. current. (c) Amperometric response of the FM/GCE to the addition of NE in the presence of interfering compounds (i.e 0.25 mM UA and 0.1 mM AA).

Table 1
Comparison of reported modified electrodes for the determination of NE with the FM/GCE produced in this study.

Electrode material	Linear range (μM)	Detection limit (μM)	Ref.
ZrO_2 nanoparticle-modified carbon paste electrode	0.1–200	0.089	(Ardakani et al., 2010)
AuNPs/ITO	0.1–25	0.0087	(Goyal et al., 2011)
WO_3–TiO_2/ITO	3.23–388	1.07	(Li et al., 2012)
CPE modified with 5-mino-3′,4′- dimethyl-biphenyl-2-ol (5ADB)	1.2–900	0.59	(Beitollahi and Mohammadi, 2013)
Molecularly imprinted polymer-coated PdNPs	0.5–80	0.1	(Chen et al., 2015)
MWCNTs/carbon ionic liquid electrode	0.3–450	0.09	(Salmanpour et al., 2012)
Molybdenum (VI) complex/carbon paste electrode	30–700	0.043	(Beitollahi and Sheikhshoaie, 2011)
$FeMoO_4$/GCE	1–200	0.0037	Present work

detection limit for NE with a wide range of concentrations.

It is well known that ascorbic acid (AA) and uric acid (UA) coexist with NE in human body fluids i.e human blood and urine, and their concentrations are always much higher than that of NE (Kazuko et al., 2003). AA and UA also oxidize at a potential near to that of NE at most electrodes, resulting in overlapping voltammetric responses. Therefore, the determination of NE in the presence of higher concentrations of AA and UA was carried out. The interference influence was investigated via the amperometry i-t curve at the FM/GCE with 15 μM NE in the presence of 0.25 mM UA and 0.1 mM AA (Fig. 5c). It was found that these common interferences, at the added concentrations did not interfere with the determination of NE. Additionally, the amperometric responses to 15 μM NE were mostly constant before and after these interferences were added. Similarly, epinephrine (E) and dopamine (DA) were also supposed to interfere in determination of NE, as both contain a catechol residue and a side-chain amine. In this study, we have used the specific oxidation potential for oxidation of NE (0.33 V). Hence, the contribution of the current from E and DA oxidation will be negligible. The high sensitivity of the electrode is due to the application of an appropriate potential and the selectivity of the as-synthesized material towards NE.

A reliable NE biosensor should show good precision (repeatability and reproducibility). The repeatability generated by the biosensor was studied by measuring the current 10 times in a single day. Aditionally, the reproducibility of the biosensor was studied by measuring the current with five different electrodes with a relative standard deviation of 3.45%. (Fig. S7). The FM/GCE was preserved in PBS (pH 7.2; 0.2 M) at room temperature after each CV measurement. It was found that the current response decreased by about 1.4% after one week (Fig. S8). The sensitivity of the FM/GCE are comparable to those of previously reported modified electrodes. These results show that the present modified electrode was very stable and reproducible for the determination of NE. This may be due to fact that the FM/GCE has good polycrystallinity, which provides an effective path for electron transport and high electrocatalytic activity.

4. Conclusions

The present study demonstrated the simple hydrothermal synthesis of $FeMoO_4$ nanorods and used as electrode materials in biosensors for the detection of NE. The synthesized electrodes exhibited excellent electrocatalytic performance towards the oxidation of NE by the formation of Fe (II)-dioxygen complexes over a wide linear concentration range (5.0×10^{-8} M and 2.0×10^{-4} M) with a detection limit as low as 3.7×10^{-9} M. This value was lower than a variety of enzyme and noble metal nanomaterial based biosensors. It was also observed that the oxidation of NE is diffusion controlled in nature with a diffusion coefficient (D) of 1.10×10^{-4} cm^2/s and a standard heterogeneous rate constant (k_s) of 4.078×10^{-3} cm/s. In the amperometric study, the FM/GCE showed a quick response (less than 3 s). Because of these remarkable analytical advantages, an effective approach for the detection of NE was established by using the as-prepared modified electrode. Our research could lead to a paradigm in future studies concerning biosensors and may lead to the preparation of actual devices.

Acknowledgement

The authors would like to acknowledge support from Basic Science Research Program (2013R1A1A2011608) funded by the Ministry of Education and Basic Research Laboratory Program (2014R1A4A1008140) through the National Research Foundation (NRF) funded by the Ministry of Science, ICT & Future Planning of Korea.

Appendix A. Supporting information

Supplementary data associated with this article can be found in the online version at http://dx.doi.org/10.1016/j.bios.2016.03.029.

References

Adams, R.N., Murrill, E., McCreery, R., Blank, L., Karolczak, M., 1972. Eur. J. Pharmacol. 17, 287–292.
Ardakani, M.M., Beitollahi, H., Amini, M.K., Mirkhalaf, F., Alibeik, M.A., 2010. Sens. Actuators B 151, 243–249.
Ardakani, M.M., Beitollahi, H., Amini, M.K., Mirkhalaf, F., Mirjalili, B.F., 2011. Biosens. Bioelectron. 26, 2102–2106.
Bard, A.J., Faulkner, L.R., 2001. Electrochemical Methods, Fundamentals and Applications. Wiley, New York.
Beitollahi, H., Sheikhshoaie, I., 2011. J. Electroanal. Chem. 661, 336–342.
Beitollahi, H., Mohammadi, S., 2013. Mater. Sci. Eng. C. 33, 3214–3219.
Bian, C., Zeng, Q., Xiong, H., Zhang, X., Wang, S., 2010. Bioelectrochem 79, 1–5.
Cai, D., Wang, D., Liu, B., Wang, Y., Liu, Y., Wang, L., Li, H., Huang, H., Li, Q., Wang, T., 2013. ACS Appl. Mater. Interfaces 5, 12905–12910.
Chen, J., Huang, H., Zeng, Y., Tang, H., Li, L., 2015. Biosens. Bioelectron. 65, 366–374.
Cherian, C.T., Reddy, M.V., Haur, S.C., Chowdari, B.V.R., 2013. ACS Appl. Mater. Interfaces 5, 918–923.
Cole, S.W., Korin, Y.D., Fahey, J.L., Zack, J.A., 1998. J. Immunol. 161, 610–616.
Cui, J.X., Wang, W.S., Zhen, L., Shao, W.Z., Che, Z.L., 2012. CrystEngComm 14, 7025–7030.
Goyal, R.N., Aziz, Md.A., Oyama, M., Chatterjee, S., Rana, A.R.S., 2011. Sens. Actuators B 153, 232–238.
Gu, H.H., Wall, S., Rudnick, G., 1996. J. Biol. Chem. 271, 6911–6916.
Harrison, J.A., Khan, Z.A., 1970. J. Electroanal. Chem. 28, 131–138.
Ju, Z.C., Zhang, E., Zhao, Y.L., Xing, Z., Zhuang, Q.C., Qiang, Y.H., Qian, Y.T., 2015. Small . http://dx.doi.org/10.1002/smll.201501294.
Kannan, P., Maiyalagan, T., Marsili, E., Ghosh, S., Jönsson, J.N., Niedziolka, M.J., 2016. Nanoscale . http://dx.doi.org/10.1039/C5NR06802A.
Kazuko, M., Hideki, K., Hiroshi, M., Toshio, O., Michael, T., 2003. Hypertens 42, 474–480.
Leyzerovich, N.N., Bramnik, K.G., Buhrmester, T., Ehrenberg, H., Fuess, H., 2004. J. Power Sources 127, 76–84.
Li, Y., Hsu, P.C., Chen, S.M., 2012. Sens. Actuators B 174, 427–435.
Liu, A.L., Zhang, S.B., Chen, W., Lin, X.H., Xia, X.H., 2008. Biosens. Bioelectron. 23, 1488–1495.

Liu, H., Gu, C., Li, D., Zhang, M., 2015. Mater. Res. Bull. 64, 375–379.
Liu, M., Kong, L., Lu, C., Li, X., Luo, L., Kang, B., 2013. Mater. Lett. 94, 197–200.
Lu, L.P., Wang, S.Q., Lin, X.Q., 2004. Anal. Chim. Acta 519, 161–166.
Mai, L.Q., Yang, F., Zhao, Y.L., Xu, X., Xu, L., Luo., Y.Z., 2011. Nat. Commun. 2, 1–5.
Nie, Z., Nijhuis, C.A., Gong, J., Chen, X., Kumachev, A., Martinez, A.W., Narovlyansky, M., Whitesides, G.M., 2010. Lab. Chip. 10, 477–483.
Oka, K., Sekiya, M., Osada, H., Fujita, K., Kato, T., Nagatsu, T., 1982. Clin. Chem. 28, 646–649.
Sabbioni, C., Saracino, M.A., Mandrioli, R., Pinzauti, S., Furlanetto, S., Gerra, G., Raggi, M.A., 2004. J. Chromatogr. A. 1032, 65–71.
Saleem, S.S., 1987. Infkred Phys. 27, 309–315.
Salmanpour, S., Tavana, T., Pahlavan, A., Khalilzadeh, M.A., Ensafi, A.A., Maleh, H.K., Beitollahi, H., Kowsari, E., Zareyee, D., 2012. Mater. Sci. Eng. C. 32, 1912–1918.
Senthilkumar, B., Selvan, R.K., Meyrick, D., Minakshi, M., 2015. Int. J. Electrochem. Sci. 10, 185–193.
Sigel, A., Sigel, H., Sigel, R.K.O., 2006. Neurodegenerative Diseases and Metal Ions: Metal Ions in Life Sciences. John Wiley and sons, pp. 291–293.
Soares, A.P.V., Portela, M.F., Kiennemann, A., Hilaire, L., Millet, J.M.M., 2001. Appl. Catal. A 206, 221–229.
Soderhjelm, E., House, M.P., Cruise, N., Holmberg, J., Bowker, M., Bovin, J.O., Andersson, A., 2008. Top. Catal. 50, 145–155.
Velasco, J.G., 1997. Electroanalysis 9, 880–882.
Wang, H.W., Wang, X.F., 2013. ACS Appl. Mater. Inter 5, 6255–6260.
Wang, J., 2008. Chem. Rev. 108, 814–825.
Wei, M., Li, M., Li, N., Gua, Z., Duan, X., 2002. Electrochim. Acta 47, 2673–2678.
Xiao, W., Chen, J.S., Li, C.M., Xu, R., Lou, X.W., 2010. Chem. Mater. 22, 746–754.
Yang, X., Zhou, Y., Yu, X., Demir, H.V., Sun, X.W., 2011. J. Mater. Chem. 21, 9009–9013.
Zhang, D., Zhang, R., Xu, C., Fan, Y., Yuan, B., 2015a. Sens. Actuators B 206, 1–7.
Zhang, G.Q., Lou, X.W., 2013. Adv. Mater. 25, 976–979.
Zhang, L., Cao, X.F., Ma, Y.L., Chen, X.T., Xue, Z.L., 2010. CrystEngComm 12, 207–210.
Zhang, W., Li, T., Kang, W., Lee, C., 2015b. J. Mater. Chem. A 3, 20527–20534.
Zhu, M., Huang, X.M., Li, J., Shen, H.X., 1997. Anal. Chim. Acta 357, 261–267.